Joint Rigid Registration of Multiple Generalized Point Sets With Hybrid Mixture Models

Zhe Min, *Student Member, IEEE*, Jiaole Wang, *Member, IEEE*, and Max Q.-H. Meng, *Fellow, IEEE*

***Abstract*— Aligning different views or representations of anatomy is an essential task in both medical imaging computing (MIC) and computer-assisted interventions' (CAIs') communities. Motivated by simultaneously registering multiple point sets (PSs) and further improving the algorithm's robustness to outliers and noise, in this paper, we propose a novel probabilistic approach to jointly register multiple generalized PSs. A generalized PS includes high-dimensional points consisting of both positional vectors and orientational information (or normal vectors). Hybrid mixture models (HMMs) combining Gaussian and von Mises–Fisher (VMF) distributions are used to model positional and orientational components of the generalized PSs. All generalized PSs are jointly registered using the expectation–maximization (EM) technique. In the E-step, the posterior probabilities representing point correspondence confidences are computed. In the M-step, the rigid transformation matrices, positional variances, and orientational concentration parameters are updated for each generalized PS. E and M steps will iterate until some termination condition is satisfied. We validate our algorithm using the surface points extracted from the human femur CT model. The experimental results demonstrate that the proposed algorithm outperforms the state-of-the-art ones in terms of the accuracy, robustness, as well as convergence speed. In addition, our algorithm is able to recover a better central PS than the state-of-the-art one does in the case of registering multiple PSs. Our algorithm is very suitable for registering complex structures arising in medical imaging.**

***Note to Practitioners*—This paper was motivated by solving the problem of registering two or multiple point sets. Most existing approaches generally use only the positional information associated with each point and thus lack robustness to noise and outliers. This paper suggests a new robust method that also adopts the normal vectors associated with each point. The registration problem is cast into a maximum-likelihood (ML) problem and solved under the expectation–maximization (EM) framework. Closed-form solutions to estimating parameters in both expectation and maximization steps are provided in this paper. We have demonstrated through extensive experiments that the proposed registration algorithm achieves improved accuracy, robustness to noise and outliers, and faster convergence speed.**

***Index Terms*— Gaussian mixture model (GMM), hybrid mixture models (HMMs), point set (PS) registration, von Mises–Fisher (VMF) distribution.**

I. Introduction

REGISTRATION of two or multiple point sets (PSs) is a fundamental problem, which has wide applications in computer vision [1], pattern recognition [1], robotics [2]–[4], computer-assisted interventions (CAIs) [5]–[7], and medical image analysis [8]–[11]. In CAIs, registration can be used to map the preoperative space to the intraoperative space [12] and also to acquire the pose of the surgical instrument [13]–[19]. In the field of medical imaging computing (MIC), registration can be used to align images from the same modality (e.g., MRI to MRI), referred to as intramodality registration, or between different modalities (e.g., MRI to CT), known as intermodality registration [20]. In the PS registration, point correspondences in two PSs are usually not known. Hard or soft assignment strategies are usually utilized to assign point correspondences. In the *hard assignment* strategy, one-to-one correspondence between points in two PSs is assumed. On the other hand, one-to-many correspondences appear in the *soft assignment* strategy.

Multiview registration is a needed step to construct the statistical shape model (SSM), which is a powerful tool in segmentation and shape analysis [10]. The multiple PSs need to be aligned to the same coordinate system. Multiview registration is usually solved by conducting pairwise registrations repeatedly, either sequentially or via a one-versus-all strategy [1]. The above-mentioned two methods have their respective significant disadvantages. First, the overall registration suffers from error propagation, while each pairwise registration is optimal locally [21]. Second, the overall registration is biased to one specific PS. In medical imaging, shapes extracted from clinical images are susceptible to corruption by outliers [22]. Spatial positions alone cannot perform well in such circumstances. In this paper, we simultaneously register multiple PSs with the assistance of normal vectors at each point.

This paper first formally defines the multiple generalized PSs' registration (MGPSR) problem and then presents a novel algorithm to solve the registration. The registration problem is formulated as a *maximum-likelihood estimation* (MLE) problem of the model parameters. Expectation–maximization (EM)

Manuscript received November 5, 2018; revised January 18, 2019; accepted March 9, 2019. Date of publication April 22, 2019; date of current version January 9, 2020. This paper was recommended for publication by Associate Editor H. Ren and Editor Y. Sun upon evaluation of the reviewers' comments. This work was supported in part by the Hong Kong RGC RGF under Grant 14210117, in part by the Hong Kong RGC NSFC RGC Joint Research Scheme under Grant CUHK448/17, and in part by the Shenzhen Science and Technology Innovation Projects Grant JCYJ20170413161616163 awarded to M. Q.-H. Meng. *(Corresponding author: Max Q.-H. Meng.)*

Z. Min is with the Department of Electronic Engineering, The Chinese University of Hong Kong, Hong Kong (e-mail: zmin@ee.cuhk.edu.hk).

J. Wang was with the Department of Electronic Engineering, The Chinese University of Hong Kong, Hong Kong. He is now with the Pediatric Cardiac Bioengineering Laboratory, Department of Cardiovascular Surgery, Boston Children's Hospital, Harvard Medical School, Boston, MA 02115 USA (e-mail: jlwang@link.cuhk.edu.hk).

M. Q.-H. Meng is with the Department of Electronic Engineering, The Chinese University of Hong Kong, Hong Kong, and also with the Shenzhen Research Institute, The Chinese University of Hong Kong, Shenzhen 518057, China (e-mail: max.meng@ieee.org).

Color versions of one or more of the figures in this article are available online at http://ieeexplore.ieee.org.

Digital Object Identifier 10.1109/TASE.2019.2906391

technique is adopted to solve the MLE problem. One point in the generalized PSs to be registered is considered to be the realizations of the unknown hybrid mixture models (HMMs). One HMM consists of a Gaussian mixture model (GMM) and a Fisher mixture model (FMM). The orientational vector of each generalized point can benefit both the E and M steps. At the beginning of our algorithm, the unknown central generalized PS is initialized in some specific manner. Points in the *central* generalized PS are considered to be the centroids of the HMMs. In the E-step, the posterior probabilities that represent the correspondence confidence between one observed point and one HMM centroid are computed. In the M steps, we update: 1) the rigid transformation matrices that align the current *central* PS to the *observed* PSs; 2) the positional variances and orientational concentration parameters associated with each of *observed* PSs; and 3) the *central* PS. Except for the concentration parameters of orientational vectors, we provide the closed-form solutions in E and M steps. We demonstrate through two experiments that our algorithm can achieve significantly better registration performances, including the accuracy, robustness, and convergence speed than the state-of-the-art methods. As a by-product, our algorithm can recover a central denoised model PS.

This paper is organized as follows. Section II reviews the related work about the PS registration. Section III illustrates the proposed algorithm in detail. Section IV describes the two experiments and presents the corresponding results. Section V discusses our algorithm and the results. Section VI concludes this paper.

II. Related Work

Registration problem can be broadly categorized into rigid registration and nonrigid registration. In terms of nonrigid registration, several important nonparametric model-based algorithms proposed by Ma *et al.* [23]–[27] recently are highlighted. They provided a uniform framework for robust feature matching called vector field consensus, which is very general and can accept various geometric models [23]. To perform PS registration, they also introduced the L_2E estimator to the matching problem [24]. They exploited both global and local geometrical structures among PSs by using shape descriptors [25] and hence enabled to deal with extreme data degeneration, such as nonrigid deformation, noise, outlier, rotation, occlusion, and so on. Moreover, a sparse approximation for solving the nonparametric model is proposed in [26]. Alternatively, they also developed an efficient approach based on maintaining the local neighborhood structures of potential true matches [27]. We mainly review both the classic and state-of-the-art rigid registration algorithms as follows.

A. Pairwise Registration

The goal of a pairwise registration is to recover the relative transformation matrix between two *PSs* (*views/scans*). Much work has been done to register two PSs.

1) ICP and Its Invariants: Iterative closest point (ICP) algorithm is the most commonly used one [9]. Two iterative steps are involved in ICP: 1) correspondence step in which the correspondences between points in two PSs are found and 2) registration step in which the best transformation matrix is updated given the current correspondences. Each step is completed by minimizing the summed distance between the points in two PSs with respect to the correspondence variables and rigid transformation matrix, respectively. There exists plenty of work to improve the ICP algorithm in various aspects [28]–[33].

Under the framework of the ICP algorithm, some work exists where normal vectors are adopted. In the iterative most likely oriented point (IMLOP) algorithm [34], the orientational information is utilized in both correspondence and registration steps. Later in the generalized IMLOP (G-IMLOP) algorithm [35], the isotropic and homogeneous assumption of both positional and orientational uncertainties is relaxed to anisotropic and inhomogeneous cases. However, the two algorithms' accuracy and robustness to outliers can be further improved, because they are still under the ICP framework.

2) Probabilistic Methods: One-to-many correspondence strategy is adopted in this category. The main idea of nearly all probabilistic methods is to represent PSs with certain probability density functions (pdfs) [36]. GMMs are frequently used to represent PSs. The rationale of using GMM is that, generally speaking, points are assumed to be corrupted by Gaussian noise. The registration problem can then be cast into a maximum-likelihood (ML) framework where the latent variables are the correspondence probabilities between the points in two PSs. The EM technique is usually used to solve the ML problem.

In the coherent point drift (CPD) method, points are assumed to move coherently over the velocity field and positional uncertainty is assumed to obey an isotropic distribution [37]. In the expectation conditional maximization for point registration (ECMPR) method, the positional uncertainty was relaxed to be anisotropic [38]. To further improve the algorithm's robustness to outliers, each Gaussian component can be given a specific weight in the asymmetrical GMM (A-GMM) method [39]. In all the above-mentioned methods, the points in one PS are assumed to be GMM centroids, while the points in the other PS are considered to be the realizations of GMM distributions. One significant disadvantage of this kind formulation is that it can cause a bias toward one PS. In the GMMReg method, both PSs are represented by GMMs and the GMM-to-GMM L_2 distance is minimized in both E and M steps [40]. One highlight in the GMMReg method is that a closed-form expression of the L_2 distance is provided and can thus lead to a computationally efficient registration algorithm.

In 2-D–3-D registrations, a few works that considers the orientation information at each 2-D point (or contour) exists [41]. A 2-D–3-D method was proposed in the context of single X-ray to CT registration [41], [42]. The 2-D orientation vectors of contours alongside with positions were modeled using the von Mises–Fisher (VMF) and Gaussian distributions [41].

Both positional and orientational data were modeled using Gaussian distributions with the aim of registering blood vessels in X-ray (2-D) and CT angiography (3-D) [42].

Under the CPD framework, we have proposed two methods for pairwise normal vector-assisted rigid registration. By utilizing the Gaussian and the VMF distributions to model the positional and orientational uncertainties, the problem of registering two PSs with normal vectors is formulated into an ML one and solved under the EM framework [43], [44]. Later, we extend the assumption of the positional error to anisotropic cases [45].

B. Multiview Registration

We classify the multiview registration algorithms into two categories: 1) sequential pairwise registration and 2) joint registration of multiple PSs. In both categories, the registration methods can be ICP-like or probabilistic ones.

1) Sequential Pairwise Registration: In a sequential pairwise registration strategy, *register-then-integrate* processes are conducted until all PSs are utilized [46]–[48]. In other words, whenever an additional set is available, the model set is updated repeatedly. The main drawback of registration methods in this category is that the registration error will accumulate.

2) Motion Averaging: Motion averaging technique [49] and rotation averaging method [50] have also been used to register multiple views (or PSs). In the motion averaging ICP (MA-ICP) algorithm, the authors use the Lie-algebraic averaging of relative motions to recover the global motions for each scan [51]. Each iteration of the MA-ICP algorithm consists of three steps as follows.

1) *Correspondence Step:* In this step, the correspondences between the points in every scan pairs are obtained given the current relative *transformation matrix/motion* between scan pairs.
2) *Motion Step:* In this step, the optimal *motion* between every scan pairs is computed given the current point correspondences.
3) *Average Step:* In this step, the relative motions are averaged to acquire the global motion for each scan.

The above-mentioned three steps iterate until convergence. Registration accuracy using the MA-ICP algorithm can be further improved due to the use of ICP in computing the relative motions. Li *et al.* [52] improve the MA-ICP in the following two aspects.

1) *Registration Accuracy:* They first present a method to estimate the overlapping percentages between scan pairs. The trimmed ICP (TR-ICP) algorithm is then applied to scan pairs with higher overlapping percentages, and then, the relative motions between those scan pairs are recovered.
2) *Registration Efficiency:* The parallel computation technique is utilized to accelerate the registration [52]. However, these methods still in some sense suffer from the disadvantages of ICP method because of their ICP-like essentials.

3) Joint Registration: Similar to [40], [49] represents each PS as a respective GMM and applies the nonrigid transformations to the multiple mixtures rather than individual points. The model parameters are estimated by minimizing the Jensen–Shannon divergence. A probabilistic mean shape is acquired by a convex combination of the already aligned sets. The main disadvantage of this method, as indicated in [21], is that it requires the PSs to be well-structured [49].

With the strict assumption of *given correspondences*, [53] iteratively reconstructs one object's mean shape and registers the views to the updated mean shape based on the EM technique. After registration, the mean shape of the object can be acquired. The most relevant and state-of-the-art registration is the *joint registration of multiple point clouds* (JRMPC) algorithm [21]. All PSs without known correspondences are regarded as independent realizations of an unknown mixture model (i.e., representing the model PS). In this way, there is no bias toward any specific PS. The model PS is initialized in a proper way. In the expectation step (E-step), the posterior probabilities are computed. Several maximization steps (M-step) exist within the JRMPC method. In the M-rigid step, the transformation matrices that align each PS to the model PS are updated.

C. Motivations and Potential Clinical Applications

As we noted earlier that under the JRMPC framework, we can have a more balanced statistical formulation toward all PSs to be registered. With the orientational information incorporated, the algorithm's accuracy and robustness to outliers can be further improved. We now summarize the sources of normal vectors or orientational information in related biomedical applications.

1) Normal Estimation: Given a PS, there exist many methods to extract the normal vectors associated with each point [54], [55]. For interested readers' references, a good summary of various surface normal estimation methods is given in [55]. One conclusion drawn from [55] is that the *PlanePCA* method is recommended among various methods. The idea of *PlanePCA* is to do the principal component analysis (PCA) of an augmented data matrix that contains the positional data of one point and its neighbors. The normal vector is taken as the *principal component* with the smallest variance after the PCA technique.

2) Normal Measurement: Oriented fiducials have also been introduced in the fiducial-based registration [56]. With the additional orientational information, only two oriented fiducials are needed to complete the registration. In surface registration, surface normal can be estimated with a tracked probe with a force/torque sensor [57], [58] or optical waveguide sensing [59].

To build a 3-D model of an object, multiple scans are needed. Generally speaking, multiview registration is to bring multiple PSs/scans/views together into a common reference coordinate frame. The SSM uses the PCA to compute a mean shape and its principal modes of variation. To construct an SSM, n instances of shapes need to be aligned to a common coordinate system [10], [60]. The clinical applications of

the proposed generalized point cloud registration algorithm include but are not limited to: 1) mapping the preoperative to intraoperative images [61], [62]; 2) reconstructing surfaces from various range images [63]; and 3) tracking the surgical tool during orthopedic surgery [63], [64]. As summarized in [65], with more enriched information (i.e., normal vectors), the generalized PS registration is particularly useful when registering shapes with complex topologies, which includes disjoint structures, holes, and bifurcations.

D. Contributions of This Paper

This paper is a significant variation of our method [43] to the cases involving multiple generalized PSs and an extension of our workshop paper [66]. The main contributions of this paper are summarized as follows.

1) The MGPSR problem is formally defined as an ML problem. One generalized point is represented by a 6-D vector that not only has positional data but also carries orientational information.
2) A novel EM-based method to jointly solve the MGPSR problem is presented. Each generalized PS is considered to own its specific model parameter (i.e., rotation matrix, translational vector, positional variance, and orientational concentration parameter).
3) The implementation details, including some practical issues of our proposed algorithm, are provided. For example, the choice of the number of hybrid mixture model's components is discussed.

III. Multiple Generalized Point Sets' Registration

This paper has the following notation conventions.

1) $N \in \mathbb{R}$ is the number of observed generalized PSs to be registered.
2) $j \in \mathbb{R}$ is the index of the observed generalized PS.
3) $i \in \mathbb{R}$ is the index of the point in each observed generalized PS.
4) $m \in \mathbb{R}$ is the index of the point in the underlying model PS.
5) $N_j \in \mathbb{R}$ is the number of points in the jth observed generalized PS.
6) $M \in \mathbb{R}$ is the number of points in the underlying model PS.
7) $q \in \mathbb{R}$ is the index of the iteration.
8) N_{trial} is the number of trials conducted in each test case.
9) $\mathbf{d}_{ji} \in \mathbb{R}^{6\times 1}$ is the ith generalized point in the jth observed generalized PS.
10) $\mathbf{d}_m \in \mathbb{R}^{6\times 1}$ is the mth generalized point in the underlying model PS.
11) $\mathbf{R}_j \in SO(3)$ is the rotation matrix that aligns the model PS with the jth observed generalized PS.
12) $\mathbf{t}_j \in \mathbb{R}^{3\times 1}$ is the translational vector that aligns the model PS with the jth observed generalized PS.
13) $\kappa_j \in \mathbb{R}$ is the concentration parameter of the VMF distribution for orientational uncertainty associated with the jth PS.
14) $\sigma_j \in \mathbb{R}^{3\times 3}$ is the the variance for the positional error associated with the jth PS.
15) $\mathbf{A}^{\mathsf{T}}$ is the transpose of a vector or a matrix $\mathbf{A}$.
16) Θ - $\Theta = (\{\mathbf{R}_j, \mathbf{t}_j, \kappa_j, \sigma_j\}_{j=1}^{N}, \{\mathbf{d}_m\}_{m=1}^{M})$ include the model parameters.
17) Θ^q - $\Theta = (\{\mathbf{R}_j^q, \mathbf{t}_j^q, \kappa_j^q, \sigma_j^q\}_{j=1}^{N}, \{\mathbf{d}_m^q\}_{m=1}^{M})$ include the model parameters that have been updated after the qth step.
18) z_{ji} is the correspondence variable.
19) $\mathbf{1}$ is a vector with all elements being one.
20) $\text{Tr}(\bullet)$ is the trace of a matrix.
21) $\text{diag}(\bullet)$ is the diagonal matrix constructed from a vector.
22) $\mathbf{D}$ is the N_j observed generalized PS.
23) $\mathbf{D}_j$ is the jth observed PS.
24) $\det(\bullet)$ is the determinant of a matrix.
25) $||\bullet||_F$ is the Frobenius norm of a matrix.
26) $\alpha_{\text{jim}} \in \mathbb{R}$ is the posterior probability that assigns the ith point in the jth observed PS to the mth point in the underlying model PS.
27) $k \in \mathbb{R}$ is the index of the registration trial.
28) GMM is the Gaussian mixture model.
29) FMM is the Fisher mixture model.
30) HMM is the Hybrid mixture model.

A. Problem Formulation

Let $\mathbf{D}_j = [\mathbf{d}_{j1}, \ldots \mathbf{d}_{ji}, \ldots \mathbf{d}_{jN_j}] \in \mathbb{R}^{6\times N_j}$ be N_j *observed generalized points* that belong to the jth PS and N be the number of PSs to be registered. More specifically, we have $\mathbf{d}_{ji} = (\mathbf{x}_{ji}; \widehat{\mathbf{x}}_{ji})$, where $\mathbf{x}_{ji} \in \mathbb{R}^{3\times 1}$ and $\widehat{\mathbf{x}}_{ji} \in \mathbb{R}^{3\times 1}$ represent the positional and orientational vectors (or normal vectors) associated with the ith generalized point in the jth PS. For clarity, we denote $\mathbf{D} = \{\mathbf{D}_j\}_{j=1}^{N}$ the union of all PSs. The aim of the MGPSR problem is to find the "best" rotation matrix set $\{\mathbf{R}_j\}_{j=1}^{N}$ and translation vector set $\{\mathbf{t}_j\}_{j=1}^{N}$ that align the *unknown central model* PS $\{\mathbf{d}_m\}_{m=1}^{M}$ to the jth observed PS. Fig. 1 summarizes the concept of the MGPSR problem.

The *observed generalized PSs* are considered to be specific realizations of an unknown M-component HMM

$$p(\mathbf{d}_{ji}) = w\frac{1}{N_j} + (1-w)\sum_{m=1}^{M}\frac{1}{M}p(\mathbf{d}_{ji}|z_{ji}=m) \tag{1}$$

where one additional *uniform distribution* $p(\mathbf{d}_{ji}|z_{ji} = M + 1) = (1/N_j)$ is added to account for noise and outliers and w denotes the weight of the uniform distribution. To summarize and for clarity, the model parameters Θ are

$$\Theta = \left(\{\mathbf{d}_m\}_{m=1}^{M}, \left\{\kappa_j, \sigma_j^2, \mathbf{R}_j, \mathbf{t}_j\right\}_{j=1}^{N}\right) \tag{2}$$

where we have defined $\mathbf{d}_m = (\mathbf{y}_m; \widehat{\mathbf{y}}_m)$, $\forall m \in [1 \ldots M]$.

We now introduce the hidden variables $\mathcal{Z} = \{z_{ji} | j \in [1, \ldots, N], i \in [1, \ldots, N_j]\}$ such that $z_{ji} = m$ indicates that the point $\mathbf{d}_{ji}$ is generated by the mth component of HMM. Gaussian and VMF distributions are utilized to model positional and orientational uncertainties, respectively. Assuming that the positional and orientational data are coindependent, the pdf of $\mathbf{d}_{ji}$ sampled from the mth component in HMM

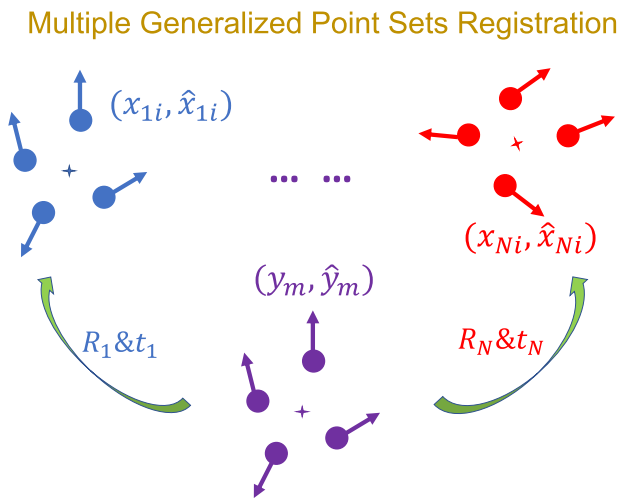

Fig. 1. Illustration of the MGPSR problem. Let N denote the number of PSs to be registered and N_j represent the number of points in the jth PS. Each generalized point in the multiple PSs consists of one positional vector $\mathbf{x}_{ji}(j \in [1 \dots N], i \in [1 \dots N_j])$ and the corresponding orientational vector $\widehat{\mathbf{x}}_{ji}$. The aim is to recover the rigid transformation matrices, which includes the rotation matrix $\mathbf{R}_j \in SO(3)$ and the translation vector $\mathbf{t}_j \in \mathbb{R}^3$ that align the jth PS and the underlying model PS. (Best viewed in color.)

whose mean is denoted as $\mathbf{d}_m$ is defined as

$$p(\mathbf{d}_{ji}|z_{ji}=m,\kappa_j,\sigma_j^2,\mathbf{R}_j,\mathbf{t}_j) = \underbrace{\frac{1}{(2\pi\sigma_j^2)^{\frac{3}{2}}}e^{-\frac{1}{2\sigma_j^2}\|\mathbf{x}_{ji}-(\mathbf{R}_j\mathbf{y}_m+\mathbf{t}_j)\|^2}}_{\text{Position}} \times \underbrace{\frac{\kappa_j}{2\pi(e^{\kappa_j}-e^{-\kappa_j})}e^{\kappa_j(\mathbf{R}_j\widehat{\mathbf{y}}_m)^{\mathsf{T}}\widehat{\mathbf{x}}_{ji}}}_{\text{Orientation}} \tag{3}$$

where κ_j and σ_j^2 represent the concentration parameter and variance associated with the jth PS, respectively, and $||\bullet||$ denotes the norm of a vector. Hereafter, let $\mathbf{Y}$ and $\widehat{\mathbf{Y}}$ denote the positional and orientational vector sets of the unknown HMM, respectively.

In order to estimate the parameters Θ, we need to maximize the *expected complete-data log-likelihood* which is defined as

$$E(\Theta|\mathbf{D},\mathcal{Z}) = \mathbb{E}_{\mathcal{Z}}[\log P(\mathbf{D},\mathcal{Z};(\Theta)|\mathbf{D}] = \sum_{\mathcal{Z}} P(\mathcal{Z}|\mathbf{D},\Theta)\log(P(\mathbf{D},\mathcal{Z};\Theta)). \tag{4}$$

Assuming that the data vectors in $\mathbf{D}$ are independent, the complete *negative log-likelihood function* is the following:

$$E(\Theta|\mathbf{D},\mathcal{Z}) = -\sum_{j=1}^{N}\sum_{i=1}^{N_j}\sum_{m=1}^{M+1}\alpha_{\text{jim}}\log P(\mathbf{d}_{ji}|z_{ji}=m;,\Theta) \tag{5}$$

where $\alpha_{\text{jim}} = p(\mathbf{d}_{ji}|z_{ji}=m)$ denotes the posterior probability. By ignoring the constants independent of Θ and utilizing the standard expressions of likelihoods [67], we can

Algorithm 1: MGPSR

Inputs: Multi-dimensional point sets $\mathbf{D} = \{\mathbf{D}_j\}_{j=1}^N$;
Outputs: $\{\mathbf{R}_j^\star, \mathbf{t}_j^\star\}_{j=1}^N$,$\{\mathbf{d}_m^\star\}_{m=1}^M$;
Initialization: Initialize the model parameters $\Theta^0 = (\{\mathbf{y}_m^0, \widehat{\mathbf{y}}_m^0\}_{m=1}^M, \{\kappa_j^0, (\sigma_j^2)^0, \mathbf{R}_j^0, \mathbf{t}_j^0\}_{j=1}^N)$;
q=1;
while *not converged* **do**
1) *E-step*: Compute α_{jim}^q using (8) given the current parameters Θ^{q-1}
2) *M-rigid step*: Update $\{\mathbf{R}_j^q, \mathbf{t}_j^q\}_{j=1}^N$ using (9) and (13)
3) *M-var step*: Update$\{(\sigma_j^2)^q, \kappa_j^q\}_{j=1}^N$ using (14) and (15)
4) *M-model step*: Update $\{\mathbf{y}_m^q, \widehat{\mathbf{y}}_m^q\}_{m=1}^M$ using (16) and (17).
5) q=q+1.
end while
return $\{\mathbf{R}_j^\star, \mathbf{t}_j^\star\}_{j=1}^N$;

rewrite (5) as

$$\begin{aligned} f(\Theta) = &-\sum_{j=1}^{N} N_{\mathbf{P}j}\log\kappa_j + \sum_{j=1}^{N} N_{\mathbf{P}j}\log(e^{\kappa_j}-e^{-\kappa_j}) \\ &-\sum_{\text{jim}}\kappa_j\alpha_{\text{jim}}(\mathbf{R}_j\widehat{\mathbf{y}}_m)^{\mathsf{T}}\widehat{\mathbf{x}}_{ji} + \frac{3}{2}\sum_{j=1}^{N} N_{\mathbf{P}j}\log\sigma_j^2 \\ &+\sum_{\text{jim}}\frac{1}{2\sigma_j^2}\alpha_{\text{jim}}||(\mathbf{x}_{ji}-\mathbf{R}_j\mathbf{y}_m-\mathbf{t}_j)||^2 \end{aligned} \tag{6}$$

where $N_{\mathbf{P}j} = \sum_{i=1}^{N_j}\sum_{m=1}^{M}\alpha_{\text{jim}}$. In order to estimate Θ, we have to solve the following *constrained* optimization problem:

$$\begin{cases} \min_\Theta \ f(\Theta) \\ \text{s.t. } \mathbf{R}_j^{\mathsf{T}}\mathbf{R}_j = \mathbf{I}, |\mathbf{R}_j| = 1, \quad \forall j \in [1 \dots N] \end{cases} \tag{7}$$

where $|\bullet|$ denotes the determinant of a matrix.

B. Expectation–Maximization Framework

Direct optimization of $f(\Theta)$ is difficult due to the induced nonlinearities by the rotation matrices. Joint registration of multiple *generalized PSs* is achieved by minimizing $f(\Theta)$ in (6) using the EM technique. At each iteration, we first estimate that in the *E-step*, the correspondence probabilities between two PSs are computed. In *M-step*, the model parameter Θ is updated. In the proposed statistical framework, each PS has its own specific variance σ_j^2 and concentration parameter κ_j for positional and orientational data. In addition, a closed-form solution to the registration problem is provided to update the rotation matrix $\mathbf{R}_j$. The proposed algorithm is summarized in Algorithm 1.

1) E-Step: In the E-step, the posterior probabilities $\alpha_{\text{jim}}^q = P(\mathbf{z}_{ji}=m|\mathbf{d}_{ji})$ are computed using Bayes' rule

$$\alpha_{\text{jim}}^q = \frac{P(\mathbf{z}_{ji}=m)p(\mathbf{d}_{ji}|\mathbf{z}_{ji}=m)}{p(\mathbf{d}_{ji})} \tag{8}$$

where $P(\mathbf{z}_{ji}=m)=(1/M)$, $p(\mathbf{d}_{ji}|\mathbf{z}_{ji}=m)$ is computed using (3) and $p(\mathbf{d}_{ji})$ is computed using (1) given the current model parameters Θ^{q-1}. The explicit detailed expression of α^q_{jim} is presented in Appendix C.

2) M-Rigid Step: This step estimates the rigid transformation (i.e., $\mathbf{R}_j$ and $\mathbf{t}_j$) that minimizes $f(\Theta)$ in (6), given current values for α^q_{jim}, $\{\mathbf{d}_m^{q-1}\}_{m=1}^M$, $\{\kappa_j^{q-1}\}_{j=1}^N$, and $\{(\sigma_j^2)^{q-1}\}_{j=1}^N$. This estimation process is conducted independently for each PS to be registered.

The rotation matrices $\{\mathbf{R}_j^q\}_{j=1}^N$ are updated by minimizing $f(\Theta)$ in (6) with respect to $\mathbf{R}_j$, subject to the two nonlinear constraints (i.e., $\mathbf{R}_j^{\mathsf{T}}\mathbf{R}_j=\mathbf{I}, |\mathbf{R}_j|=1$)

$$\mathbf{R}_j^q=\arg\min_{\mathbf{R}_j}\left(-\underbrace{\sum_{i=1}^{N_j}\sum_{m=1}^{M}\frac{1}{(\sigma_j^2)^{q-1}}\alpha^q_{\text{jim}}((\mathbf{x}'_{ji})^q)^{\mathsf{T}}\mathbf{R}_j(\mathbf{y}'_{m,j})^q}_{\mathbf{H}^q_{1j}}+\underbrace{\sum_{i=1}^{N_j}\sum_{m=1}^{M}\kappa_j^{q-1}\alpha^q_{\text{jim}}(\mathbf{R}_j\widehat{\mathbf{y}}_m)^{\mathsf{T}}\widehat{\mathbf{x}}_{ji}}_{\mathbf{H}^q_{2j}}\right) \tag{9}$$

where we only retain the terms that are related to $\mathbf{R}_j$ in (6), $(\mathbf{x}'_{ji})^q=\mathbf{x}_{ji}-\boldsymbol{\mu}^q_{x,j}$ and $(\mathbf{y}'_{m,j})^q=\mathbf{y}_m-\boldsymbol{\mu}^q_{y,j}$. We have defined $\boldsymbol{\mu}^q_{x,j}$ and $\boldsymbol{\mu}^q_{y,j}$, respectively, as follows:

$$\boldsymbol{\mu}^q_{x,j}=\frac{\sum_{i=1}^{N_j}\sum_{m=1}^{M}\alpha^q_{\text{jim}}\mathbf{x}_{ji}}{N^q_{\mathbf{P}j}} \tag{10}$$

$$\boldsymbol{\mu}^q_{y,j}=\frac{\sum_{i=1}^{N_j}\sum_{m=1}^{M}\alpha^q_{\text{jim}}\mathbf{y}_m^{q-1}}{N^q_{\mathbf{P}j}} \tag{11}$$

where $N^q_{\mathbf{P}j}=\sum_{i=1}^{N_j}\sum_{m=1}^{M}\alpha^q_{\text{jim}}$. Let $\mathbf{H}^q_j=\mathbf{H}^q_{1j}+\mathbf{H}^q_{2j}$, $\forall j\in[1\ldots N]$, and after doing singular value decomposition (SVD) of $\mathbf{H}^q_j$ (i.e., $\mathbf{H}^q_j=\mathbf{U}^q_j\mathbf{S}^q_j(\mathbf{V}^q_j)^{\mathsf{T}}$), we can compute $\mathbf{R}^\star_j$ as

$$\mathbf{R}^q_j=\mathbf{V}^q_j\ \text{diag}\left(\left[1,1,\det\left(\mathbf{V}^q_j(\mathbf{U}^q_j)^{\mathsf{T}}\right)\right]\right)\ \left(\mathbf{U}^q_j\right)^{\mathsf{T}}. \tag{12}$$

The detailed derivations of (12) are presented in Appendix D. Now, we update the translation vectors $\{\mathbf{t}_j\}_{j=1}^N$ by solving $\partial f(\Theta)/\partial\mathbf{t}_j=\mathbf{0}, \forall j\in[1,\ldots,N]$

$$\mathbf{t}^q_j=\frac{\sum_{i=1}^{N_j}\sum_{m=1}^{M}\alpha^q_{\text{jim}}\mathbf{x}_{ji}-\sum_{i=1}^{N_j}\sum_{m=1}^{M}\alpha^q_{\text{jim}}\mathbf{R}^q_j\mathbf{y}_m^{q-1}}{N^q_{\mathbf{P}j}}. \tag{13}$$

We should notice that $\mathbf{t}^q_j$ is only up to the positional vectors in the *observed* and *model* PSs.

3) M-Var Step: This step estimates the positional variances $\{(\sigma_j^2)^q\}_{j=1}^N$ for positional data and concentration parameters $\{\kappa_j^q\}_{j=1}^N$ for orientational data, given current values for posteriors α^q_{jim}, the current rigid transformation $\{\mathbf{R}^q_j,\mathbf{t}^q_j\}_{j=1}^N$, and the underlying model set $\{\mathbf{d}_m^{q-1}\}_{m=1}^M$.

First, the GMM positional variances $\{\sigma_j^2\}_{j=1}^N$ are updated by solving $\partial f(\Theta)/\partial\sigma_j^2=0, \forall j\in[1\ldots N]$

$$\left(\sigma_j^2\right)^q=\frac{\sum_{i=1}^{N_j}\sum_{m=1}^{M}\left\|\mathbf{x}_{ji}-\left(\mathbf{R}^q_j\mathbf{y}_m+\mathbf{t}^q_j\right)\right\|^2}{3N^q_{\mathbf{P}j}}. \tag{14}$$

We should notice again that, in (14), the updated variance $(\sigma_j^2)^q$ is only up to the positional information.

Given the current values for posteriors α^q_{jim} and the current rigid transformations $\{\mathbf{R}^q_j,\mathbf{t}^q_j\}_{j=1}^N$, the concentration parameters $\{\kappa_j^q\}_{j=1}^N$ are updated by solving $\partial f(\Theta)/\partial\kappa_j=0, \forall j\in[1\ldots N]$

$$\frac{1}{\kappa_j}=\frac{e^{\kappa_j}+e^{-\kappa_j}}{e^{\kappa_j}-e^{-\kappa_j}}-\frac{1}{N^q_{\mathbf{P}j}}\sum_{i=1}^{N_j}\sum_{m=1}^{M}\alpha^q_{\text{jim}}\left(\mathbf{R}^q_j\widehat{\mathbf{y}}_m\right)^{\mathsf{T}}\widehat{\mathbf{x}}_{ji} \tag{15}$$

where the *fixed point iteration* method is used to solve the above-mentioned nonlinear equation of κ_j.

4) M-Model Step: This step estimates the GMM means/centroids $\{\mathbf{y}^q_m\}_{m=1}^M$ and FMM *central directions* $\{\widehat{\mathbf{y}}^q_m\}_{m=1}^M$, given the current estimates of posteriors α^q_{jim}, the rigid transformations $\{\mathbf{R}^q_j,\mathbf{t}^q_j\}_{j=1}^N$, positional variances $\{(\sigma_j^2)^q\}_{j=1}^N$, and concentration parameters $\{\kappa_j^q\}_{j=1}^N$.

The GMM means $\{\mathbf{y}^q_m\}_{m=1}^M$ are updated by solving $\partial f(\Theta)/\partial\mathbf{y}_m=\mathbf{0}, \forall m\in[1,\ldots,M]$, which yields

$$\mathbf{y}^q_m=\frac{\sum_{i=1}^{N_j}\sum_{j=1}^{N}\frac{1}{\left(\sigma_j^2\right)^q}\alpha^q_{\text{jim}}\left(\mathbf{R}_j^{q\mathsf{T}}\mathbf{x}_{ji}-\mathbf{R}_j^{q\mathsf{T}}\right)}{N_{\mathbf{P}m}} \tag{16}$$

where $N_{\mathbf{P}m}=\sum_{j=1}^{N}\sum_{i=1}^{N_j}\alpha^q_{\text{jim}}(1/(\sigma_j^2)^q)$.

The FMM central directions $\{\widehat{\mathbf{y}}^q_m\}_{m=1}^M$ are updated by maximizing $\mathbf{H}_{2j}$ in (9) with respect to $\widehat{\mathbf{y}}_m$ subject to $||\widehat{\mathbf{y}}_m||=1$, $\forall m\in[1,\ldots,M]$, and we can get

$$\widehat{\mathbf{y}}^q_m=\frac{\sum_{i=1}^{N_j}\sum_{j=1}^{N}\kappa_j^q\alpha^q_{\text{jim}}\mathbf{R}_j^{q\mathsf{T}}\widehat{\mathbf{x}}_{ji}}{\left\|\sum_{i=1}^{N_j}\sum_{j=1}^{N}\kappa_j^q\alpha^q_{\text{jim}}\mathbf{R}_j^{q\mathsf{T}}\widehat{\mathbf{x}}_{ji}\right\|}. \tag{17}$$

C. Implementation and Initialization Details

As the registration algorithm iterates, the variance σ_j^2 will become smaller, while the concentration parameter κ_j will become larger. When the posterior probability $P(\mathbf{z}_{ji}=m|\mathbf{d}_{ji})$ is computed using (8), κ_j cannot be too large to make e^{κ_j} computable. Empirically, we set the upper bound for all κ_j as 70. The criterion for the EM steps to terminate includes the following: 1) the number of iterations reaches 100; 2) the largest change of σ_j^2 is less than 10^{-8}; and 3) the largest σ_j^2 is less than 10^{-5}. All the methods were implemented in MATLAB (R2017b, MathWorks).

We now describe the proper initializations of the model parameters $\Theta^0=(\{\mathbf{y}^0_m,\widehat{\mathbf{y}}^0_m\}_{m=1}^M,\{\kappa_j^0,(\sigma_j^2)^0,\mathbf{R}^0_j,\mathbf{t}^0_j\}_{j=1}^N)$. All the rotation matrices are initialized to be the identity matrix, i.e., $\mathbf{R}^0_j=\mathbf{I}_3, \forall j\in[1,\ldots,N]$. The translation vectors are initialized to be the centroid difference between one observed PS and the model PS as the authors done in [21], i.e., $\mathbf{t}^0_j=\overline{\mathbf{x}}_j-\overline{\mathbf{y}}$, where $\overline{\mathbf{y}}$ is the GMMs' centroid and $\overline{\mathbf{x}}_j$

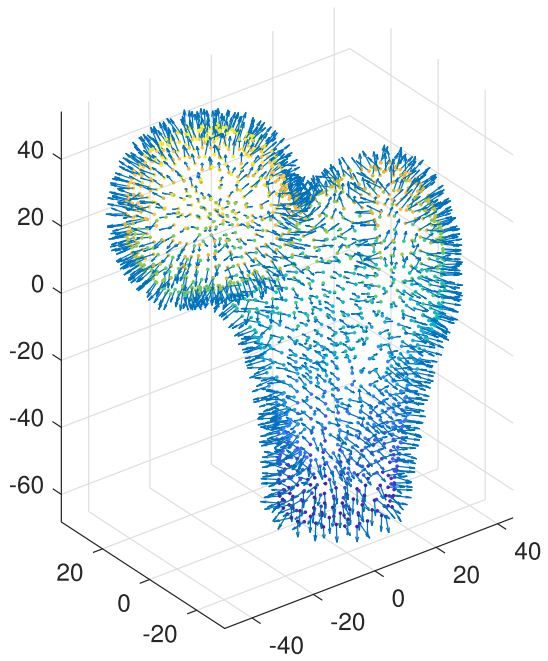

Fig. 2. Femur bone model point with positional vectors represented by points and the normal vectors represented by arrows.

is the positional centroid of the jth generalized PS $\mathbf{D}_j$. The positional variance $(\sigma_j^2)^0$ is initialized to be large, while the concentration parameter κ_j^0 is initialized to be rather small. The rationale behind this is that at the beginning of EM steps, the error values associated with both the positional and the orientational information are quite large. In this paper, $(\sigma_j^2)^0$ is empirically set to be 1000, while κ_j^0 is set to be 10, $\forall j \in [1 \ldots N]$. The initialization of $\{\mathbf{y}_m^0\}_{m=1}^M$ is the same as that in [21]. The number of HMM components M is set to be 450. To initialize $\{\widehat{\mathbf{y}}_m\}_{m=1}^M$, we first generate M vectors whose single vector element obeys the zero-mean (with 1 deg standard deviation) Gaussian distribution. Then, we normalize all vectors to produce the normal vectors $\{\widehat{\mathbf{y}}_m\}_{m=1}^M$.

IV. Experiments and Results

To verify the proposed algorithm, two experiments are conducted. We use the surface points extracted from the CT scan of the human femur model (see Fig. 2) [34]. The normal vectors associated with each 3-D point in the human femur PS were extracted using the PCA technique. The human femur model PS (i.e., $\mathbf{D}_2$) consists of $N_2 = 1568$ *generalized points*. In Experiment I, two PSs are registered, which we refer to the problem as the pairwise registration. In Experiment II, four PSs are registered, which we refer to the problem as the multiview registration.

A. Experiment I: Pairwise Registration

The *observed PS* $\mathbf{D}_1$ is first generated by random sampling $N_1 = 100$ points from $\mathbf{D}_2$. Positional and orientational error vectors are added into $\mathbf{D}_1$ to generate the *disturbed* $\mathbf{D}_1$. Correspondingly, the error vectors are randomly generated according to Gaussian with $\sigma^2 = (1/3)$ mm and VMF distributions with $\kappa = 3200$. To test the robustness of the proposed algorithm with respect to outliers, outlier points (with normal vectors randomly sampled from $[0, 360]^\circ$) are further added in the *disturbed* $\mathbf{D}_1$. Five levels of percentages of outliers are tested (i.e., $10\%, 30\%, 50\%, 70\%, and 90\%$). More specifically, $N_1 \times 10\% = 10$ additional outlier points are injected into the *disturbed* PS $\mathbf{D}_1$ when there are 10% outliers. We denote one test case as one with specific noise level and specific percentage of outliers injected. For each test case, $N_{\text{trial}} = 30$ registration trials are conducted. In the kth ($k = 1, \ldots, N_{\text{trial}}$) registration trial, the "true" rigid transformation matrix $[\mathbf{R}_{\text{true}}^k, \mathbf{t}_{\text{true}}^k]$ was generated by randomly selected from $[10, 20]^\circ$ and $[10, 20]$ mm. Then, the generated transformation matrix $[\mathbf{R}_{\text{true}}^k, \mathbf{t}_{\text{true}}^k]$ is applied to $\mathbf{D}_2$ to generate the *misaligned* $\mathbf{D}_2$ with respect to the first PS $\mathbf{D}_1$. In one registration trial, the *misaligned* $\mathbf{D}_2$ are registered to the *disturbed* $\mathbf{D}_1$ to recover the rigid transformation $[\mathbf{R}_{\text{cal}}, \mathbf{t}_{\text{cal}}]$ using all test algorithms. More specifically, in a pairwise registration and using our algorithm, the recovered rotation matrix between two PSs is computed as $\mathbf{R}_{\text{cal}}^k = (\mathbf{R}_{\text{cal},1}^k)^\mathsf{T} \mathbf{R}_{\text{cal},2}^k$, where $\mathbf{R}_{\text{cal},1}^k$ and $\mathbf{R}_{\text{cal},2}^k$ are the computed (*calculated*) rotation matrices that align the underlying *central* PSs with the $\mathbf{D}_1$ (*observed*) and $\mathbf{D}_2$ (*model*) PSs in the kth registration trial, respectively. The registration accuracy using our algorithm is compared to those using ICP [68], JRMPC [21], and ECMPR [38] methods. The rotational error value in the kth registration trial is computed as follows:

$$\mathbf{R}_{\text{err}}^k = \left\| \mathbf{R}_{\text{cal}}^k - \mathbf{R}_{\text{true}}^k \right\|_F \tag{18}$$

where $||\bullet||_F$ stands for the Frobenius norm of a matrix. Only the mean and standard deviation of the rotational errors are recorded, since computing/recovering the translation vector is not challenging [21].

1) Error Exists in One Point Set: In this section, the *misaligned* $\mathbf{D}_2$ is the *model* PS without noise injected. Table I shows the rotational error's statistics (i.e., mean and standard deviation).[1] Several observations can be made from Table I: 1) ICP and JRMPC perform worse with more outliers; 2) ECMPR and our algorithm's performances are robust with respect to different percentages of outliers; and 3) our algorithm achieves the smallest error values among the four algorithms in all test cases. For example, we achieved $\mathbf{R}_{\text{err}} = 0.0278 \pm 0.0242$, while JRMPC achieved $\mathbf{R}_{\text{err}} = 0.0917 \pm 0.0828$ in the last test case with 90% outliers. We should also note that our proposed algorithm in this paper performs similar (i.e., no significant difference) to that in [43] in this case. Fig. 3(a) shows the rotational error values with iterations using the four registration methods in one random registration trial.

2) Error Exists in Two Point Sets: In this section, error vectors are also injected into the *misaligned* $\mathbf{D}_2$ in addition to $\mathbf{D}_1$.[2] Thus, both *misaligned and disturbed* $\mathbf{D}_2$ and *disturbed* $\mathbf{D}_1$ are

[1] For example, using one specific registration algorithm, the mean value $\mu_{rot,error}$ of the rotational error in F-norm in one specific test case is computed as: $\mu_{\text{rot,error}} = (\sum_{k=1}^{N_{\text{trial}}} \mathbf{R}_{\text{err}}^k / N_{\text{trial}})$. On the other hand, the standard deviation of the rotational error in the corresponding case is $\sigma_{\text{rot,error}} = (\sum_{k=1}^{N_{\text{trial}}} (\mathbf{R}_{\text{err}}^k - \mu_{\text{rot,error}})^2 / (N_{\text{trial}} - 1))^{1/2}$.

[2] Note that the outliers only exist in the *disturbed* $\mathbf{D}_1$.

TABLE I

ROTATIONAL ERRORS USING ICP, JRMPC, ECMPR AND THE PROPOSED ALGORITHM. DIFFERENT PERCENTAGES OF OUTLIERS AND ISOTROPIC NOISE VECTORS ARE INJECTED INTO $\mathbf{D}_1$

Registration Methods	10%	30%	50%	70%	90%
ICP	0.0632±0.0496	0.1284±0.1024	0.1942±0.1046	0.1772±0.0982	0.2013±0.1051
JRMPC	0.0322±0.0195	0.0330±0.0264	0.0451±0.0364	0.0813±0.0710	0.0917 ±0.0828
ECMPR	0.0439±0.0208	0.0416±0.0203	0.0389±0.0170	0.0393±0.0176	0.0369±0.0176
Proposed Method	**0.0265±0.0147**	**0.0255±0.0208**	**0.0225±0.0118**	**0.0250±0.0125**	**0.0278±0.0242**

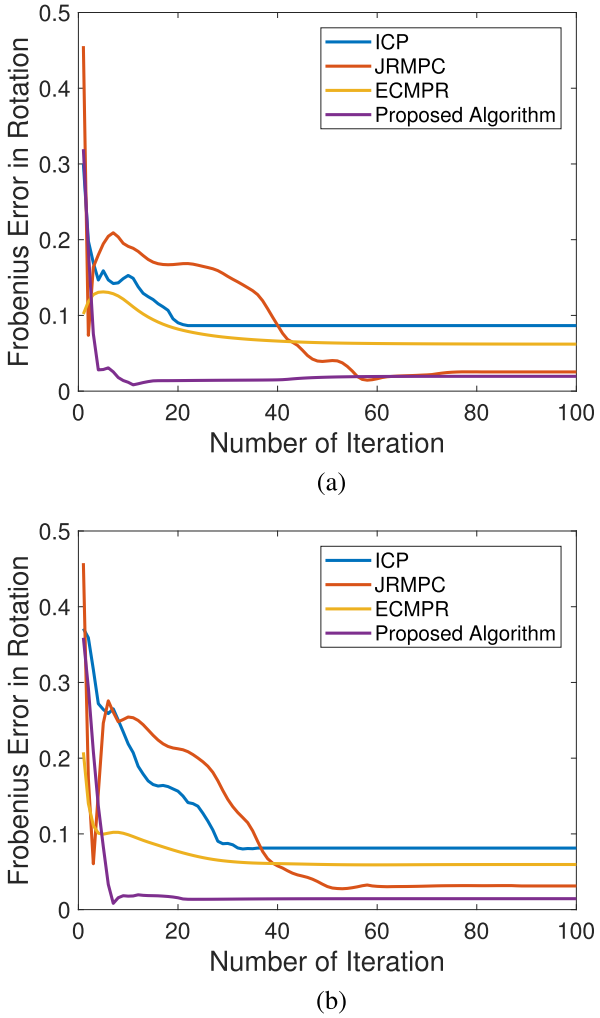

Fig. 3. Convergence speed of rotational error using the four algorithms in one random trial when 10% outliers are added in $\mathbf{D}_1$. (a) Error exists in one PS $\mathbf{D}_1$. (b) Error exists in both PSs $\mathbf{D}_1$ and $\mathbf{D}_2$.

now considered as *observed* PS. For each registration trial, we are registering *misaligned and disturbed* $\mathbf{D}_2$ with *disturbed* $\mathbf{D}_1$. Table II summarizes the corresponding rotation errors. Similar observations can be made such as those in Table I. Comparing the results in Tables I and II, we can conclude that all algorithms achieve larger rotational error when noise exists in both PSs. Fig. 3(b) shows the rotational error values with iterations using the four registration methods in one random registration trial.

To verify that the experimental results are statistically significant, we report the p-value of one tailed paired t-test ($\alpha = 0.05$) for two levels of noise in Table III. As it is shown in Table III, most of the p-values are less than 0.05. For instance, the p-value between the algorithms in our method and JRMPC for the case of 70% outliers under the low level of noise (noise exists in one PS) is 1.8749×10^{-4}, which is very small. The small p-values indicate that most of the results achieved by different methods are statistically significant and have not occurred by chance. However, we should notice that when noise exists in both PSs, the differences of performances using ECMPR and our algorithm are not statistically significant (at the 5% significance level).

B. Experiment II: Multiple Point Sets' Registration

In this section, $N = 4$ PSs (i.e., $\{\mathbf{D}_j\}_{j=1}^N$) are aligned together. Each PS has its own numbers of points, i.e., $N_1 = 1000$, $N_2 = 100$, $N_3 = 200$, and $N_4 = 300$. The number of components in the underlying *central* HMM, M, is set to be the mean cardinality, namely, $M = 400$ in our case. Among the four PSs $\{\mathbf{D}_j\}_{j=1}^N$, the first PS $\mathbf{D}_1$ is regarded as the reference PS in the evaluation process. In the kth registration trial, the "true" rigid transformation matrices $\{[\mathbf{R}_{\text{true},j}^k, \mathbf{t}_{\text{true},j}^k]\}_{j=2}^N$ associated with the jth PS were generated by randomly and uniformly selected in $[0, 10]^\circ$ and $[0, 10]$ mm. The *misaligned* $\{\mathbf{D}_j\}_{j=2}^N$ are further acquired using$\{[\mathbf{R}_{\text{true},j}^k, \mathbf{t}_{\text{true},j}^k]\}_{j=2}^N$. To test the algorithm's robustness to noise and outliers, noise vectors and outlier generalized points are injected into $\mathbf{D}_1$ and *misaligned* $\{\mathbf{D}_j\}_{j=2}^N$.[3] Two levels of noise are tested. In the case of low-level noise, the positional and orientational error vectors are generated in a similar way as those in Experiment I and are injected into all four PSs $\{\mathbf{D}_j\}_{j=1}^N$. In the case of high-level noise, the positional variance $\sigma^2 = (4/3)$ and the concentration parameter $\kappa = 800$ are used to generate the corresponding noise vectors. Nine different percentages of outliers are further injected into $\mathbf{D}_1$ and *misaligned* $\{\mathbf{D}_j\}_{j=2}^N$ (i.e., 10%–90% with 10% interval). More specifically, $N_1 \times 10\% = 100$ outlier points are injected into the *misaligned* $\mathbf{D}_1$ when there are 10% outliers. The first PS is called as *disturbed* $\mathbf{D}_1$,[4] while the other three PSs are called as *misaligned and disturbed* $\{\mathbf{D}_j\}_{j=2}^N$. Then, the four PSs (i.e., *disturbed* $\mathbf{D}_1$ and *misaligned and disturbed* $\{\mathbf{D}_j\}_{j=2}^N$) are simultaneously registered using JRMPC [21] and our algorithm. With our algorithm, the estimated rotation matrices that align $\mathbf{D}_2, \mathbf{D}_3$, and $\mathbf{D}_4$ to $\mathbf{D}_1$ are computed as $\mathbf{R}_{\text{cal},1}^{\mathsf{T}}\mathbf{R}_{\text{cal},j}$, for $j = 2, 3, 4$,

[3]We should note that we are injecting noise and outliers after we misalign the PSs.

[4]Since the first PS $\mathbf{D}_1$ is not misaligned before registration.

TABLE II

ROTATIONAL ERRORS USING ICP, JRMPC, ECMPR, AND THE PROPOSED ALGORITHM. DIFFERENT PERCENTAGES OF OUTLIERS ARE INJECTED INTO $\mathbf{D}_1$, WHILE ISOTROPIC NOISE VECTORS ARE INJECTED INTO BOTH $\mathbf{D}_1$ AND $\mathbf{D}_2$

Registration Methods	10%	30%	50%	70%	90%
ICP	0.0839±0.0586	0.1281±0.0782	0.2011±0.0984	0.1899±0.0937	0.1985±0.0946
JRMPC	0.0416±0.0208	0.0589±0.0548	0.0478±0.0388	0.0823±0.0633	0.1060±0.0882
ECMPR	0.0463±0.0230	**0.0443±0.0234**	0.0417±0.0212	0.0413±0.0202	0.0398±0.0211
Proposed Method	**0.0397±0.0222**	0.0444±0.0273	**0.0396±0.0237**	**0.0395±0.0211**	**0.0386±0.0193**

TABLE III

p-VALUE OF THE STATISTICAL TESTS COMPARING THE ROTATIONAL ERROR VALUES USING ICP, JRMPC, AND ECMPR WITH THOSE USING OUR PROPOSED ALGORITHM IN EXPERIMENT I

	Noise exists in the observed point set			Noise exists in observed and model point sets		
Outlier Percentage	ICP	JRMPC	ECMPR	ICP	JRMPC	ECMPR
10%	4.0341×10^{-04}	**0.2945**	4.0949×10^{-04}	0.0011	**0.8843**	**0.2292**
30%	1.0943×10^{-05}	**0.0697**	6.8582×10^{-05}	1.5541×10^{-06}	0.0253	**0.0696**
50%	1.1667×10^{-09}	0.0012	0.0119	2.2292×10^{-09}	0.0382	**0.7839**
70%	1.1377×10^{-09}	1.874910^{-04}	0.0015	4.6814×10^{-10}	4.6681×10^{-04}	**0.0708**
90%	6.2681×10^{-10}	7.9457×10^{-04}	1.8516×10^{-04}	7.7867×10^{-10}	0.0016	**0.8416**

where $\mathbf{R}_{\text{cal},j}\,(j=1,2,3,4)$ are the rotation matrices that align the *central* model PS with each *observed* PS. The rotational error value in the kth registration trial is calculated as follows:

$$\mathbf{R}^k_{\text{err},j} = \left\| \left(\mathbf{R}^k_{\text{cal},1}\right)^{\mathsf{T}} \mathbf{R}^k_{\text{cal},j} - \mathbf{R}^k_{\text{true},j} \right\|_F \tag{19}$$

where $j=2,3,4$. The rotational error values associated with the latter three views $\{\mathbf{R}^k_{\text{err},j}\}_{j=2}^N$ are recorded. The registration accuracy using the proposed algorithm is compared to that using JRMPC [21].

In Fig. 4, we plot the integrated *central* model PS in the case of 10% and 30% outliers. Comparing Fig. 4(a) and (b), we can see that our algorithm is able to acquire a better integrated model. Comparing Fig. 4(a) and (c), we can conclude that the JRMPC method's ability to recover the *central* model PS decreases with more outliers. On the other hand, looking carefully at Fig. 4(b) and (d), we can conclude that our algorithm can acquire a rather good model in both cases of outliers.

Fig. 5(a) and (b) shows the rotational error *root-mean-square (rms)* values [5] for $\{\mathbf{D}_j\}_{j=2}^N$ with different percentages of outliers under low and high levels of noise, respectively. As it is shown in both plots of Fig. 5, with the JRMPC method, the rotational errors associated with $\mathbf{D}_2$ and $\mathbf{D}_4$ are the largest and smallest among the three PSs, respectively. With our algorithm, as it can be seen from both plots in Fig. 5, the rotational error value associated with $\mathbf{D}_2$ is larger than those associated with $\mathbf{D}_3$ and $\mathbf{D}_4$ that have no evident difference. The higher registration accuracy of $\mathbf{D}_4$ compared with $\mathbf{D}_2$ and $\mathbf{D}_3$ using both algorithms can be easily understood since we have more points in $\mathbf{D}_4$. For all the latter three PSs $\{\mathbf{D}_j\}_{j=2}^N$, the rotational error values using our algorithm are less than those using the JRMPC method for both levels of noise. Comparing Fig. 5(a) with (b), the rotational errors of all three PSs $\{\mathbf{D}_j\}_{j=2}^N$ using both algorithm increase with larger noise. Fig. 5(c) shows the mean rotational error *rms* values of $\{\mathbf{D}_j\}_{j=2}^N$ using the two algorithms. As it is shown in Fig. 5(c), our algorithm achieves a lower rotational error with both levels of noise. It is again clearly shown that our algorithm is greatly robust to more injected outliers.

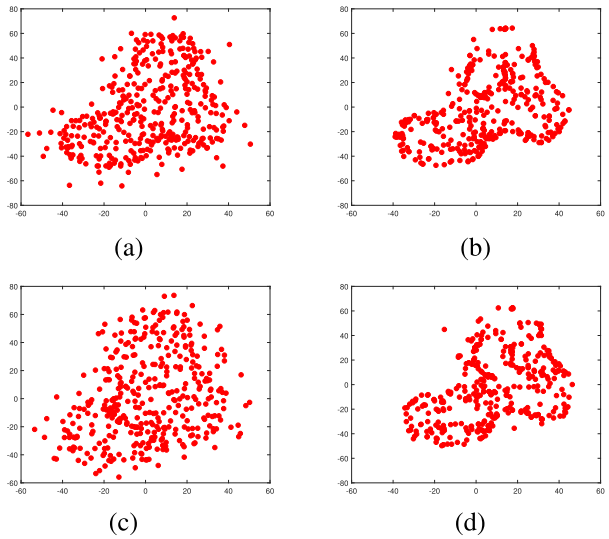

Fig. 4. Integrated positional model recovered using (a) JRMPC and (b) our algorithm when 10% outliers are injected in all PSs. The integrated positional model recovered using (c) JRMPC and (d) our algorithm when 30% outliers are injected in all PSs.

To verify that the experimental results are statistically significant, we report the p-value, called one-tailed paired t-test ($\alpha = 0.05$) for two levels of noise in Table IV.

As it is shown in Table IV, most of the p-values are less than 0.05. For instance, the p-value between the algorithms in our method and JRMPC for the case of 50% outliers under low

[5]The rms value associated with the $\mathbf{D}_j$ is computed as $\text{rms}_{\text{error},j} = \sum_{k=1}^{N_{\text{trial}}} (\mathbf{R}^k_{\text{err},j})^2 / N_{\text{trial}}{}^{1/2}$.

TABLE IV

p-VALUE OF THE STATISTICAL TESTS COMPARING THE ROTATIONAL ERROR VALUES USING ICP, JRMPC, AND ECMPR WITH THOSE USING OUR PROPOSED ALGORITHM IN EXPERIMENT II

	Low Noise			High Noise		
Outlier Percentage	View 2	View 3	View 4	View 2	View 3	View 4
10%	0.0229	0.0271	**0.0965**	0.0082	**0.4005**	**0.7694**
20%	0.0014	0.0993	**0.0071**	1.17E-04	**0.1095**	**0.8756**
30%	0.0016	0.0094	0.0465	0.0025	**0.1268**	**0.4968**
40%	0.0034	3.18×10^{-04}	0.0053	7.86×10^{-05}	0.0270	**0.9743**
50%	0.0012	1.26×10^{-04}	8.69×10^{-05}	0.0016	0.0430	**0.0984**
60%	0.0012	0.0022	3.00×10^{-04}	0.0113	0.0136	**0.9580**
70%	5.52×10^{-05}	1.80×10^{-04}	8.31×10^{-05}	0.0022	0.0079	**0.6398**
80%	3.37×10^{-06}	5.71×10^{-06}	3.93×10^{-06}	1.47×10^{-04}	0.0368	**0.2303**
90%	4.56×10^{-04}	1.91×10^{-06}	7.56×10^{-06}	2.00×10^{-06}	**0.1346**	**0.2863**

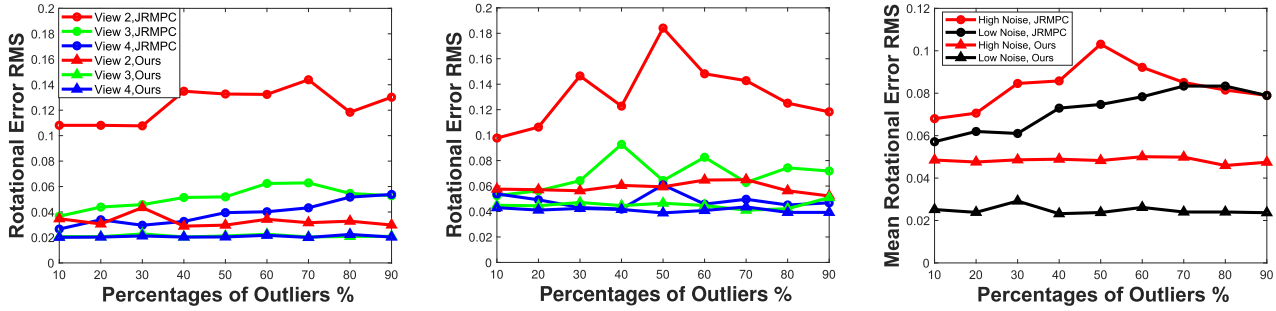

Fig. 5. Rotational error rms values of views 2–4 $\{\mathbf{D}_j\}_{j=2}^{N}$ using both JRMPC and our algorithm when different percentages of outliers are injected in all views. (a) Low level of noise and (b) high level of noise are also injected in all views. (c) Mean rotational error rms values of views 2–4 $\{\mathbf{D}_j\}_{j=2}^{N}$ using both JRMPC and our algorithm when different percentages of outliers are injected in all PSs.

level of noise is 8.27×10^{-10}, which is very small. The small p-values indicate that most of the results achieved by different methods are statistically significant and have not occurred by chance. We should notice that for $\mathbf{D}_4$, the differences of performances using JRMPC and our algorithm are not statistically significant (at the 5% significance level).

V. DISCUSSION

In this paper, multiple PSs are jointly registered with the orientational information utilized. Our algorithm is indeed a significant extension of the state-of-the-art JRMPC method [21]. The orientational information is adopted in both expectation and maximization steps. In other words, the orientational information can benefit both point correspondence and registration steps. Our algorithm can be used to solve both *pairwise* and *multiple* PS registration problems. As shown in the results of Experiment I, in pairwise registration, our algorithm is more accurate, is more robust, and 3) converges much faster than the other algorithms. As shown in the results of Experiment II, our algorithm can also recover a more accurate integrated model than JRMPC does.

In our algorithm, each PS (*view* or *scan*) $\mathbf{D}_j$ is assumed to own its specific model parameters. As it is shown in (9) and (13)–(15), the model parameters associated with the jth PS are updated using only the positional and orientational vectors in $\mathbf{D}_j$. Doing this can leave more flexibility in the case of multimodal registration where the positional and orientational uncertainties are usually not the same among different scans. On the other hand, the *central* model PS is updated using all the positional and orientational data of all PSs, as shown in (16) and (17). In other words, the information associated with all PSs contributes to recover the *central* PS.

With the assumption of isotropic positional and orientational uncertainties, closed-form solutions of updating the rotation matrix and translation vector can be derived in the M-rigid step. This leads to fast computational speed of our algorithm. We note that in (9), both the positional and the orientational information of $\mathbf{D}$ and *central* PSs contribute to update the rotation matrix $\{\mathbf{R}_j^q\}_{j=1}^{N}$. This characteristic can explain the higher registration accuracy of our algorithm than that of JRMPC since more enriched information is utilized. We also find that both the positional and the orientational information are used to compute the posterior probabilities α_{jim}, taking a careful look into (3) and (8). This characteristic can explain the great robustness of our algorithm with respect to a large number of outliers. To summarize, the enriched orientation information can benefit both the expectation and maximization steps.

Our algorithm is some sense a significance extension of JRMPC to the *high-dimensional* (six) PS registration problem. The main distinctions of our algorithm are summarized as follows.

1) The normal vector along with the positional one at each point is utilized. As we have shown in Section IV, our algorithm can achieve significantly improved performances.
2) In JRMPC, the *observed* PSs are aligned to the *central* one, while in ours, the *central* PS is aligned to the *observed* ones. This difference can be easily seen by observing (12).
3) In JRMPC, each GMM component owns its positional variance value, while in ours, each *observed* PS has its specific positional variance and orientational concentration parameter. With the normal vectors utilized, our algorithm can achieve a better performance than the JRMPC.

Various possible extensions of our algorithm are now summarized as follows. First, the HMM components can be weighted to further improve the algorithm's robustness [39]. Furthermore, each HMM component can be assumed to be the combinations of multiple weighted kernels to further improve the performance [69]. Second, the isotropic assumptions of both positional and orientational uncertainties can be relaxed to anisotropic ones [45]. The anisotropic characteristic of the positional noise can come from using the stereo camera to do the surface reconstruction.

VI. Conclusion

We have proposed a novel probabilistic method to register together multiple PSs with normal vectors. The proposed method that is tailored for multiple PSs' registration problem can also be used in pairwise registrations. The results in the pairwise registrations demonstrate that our algorithm can achieve higher registration accuracy with faster convergence speed and more robustness with respect to outliers than the state-of-the-art algorithms can. Compared with the JRMPC method, in the case of multiple PSs registration, our algorithm is able to recover a better model PS. The results also demonstrated the robustness of our method to the presence of a large amount of outliers.

Appendix A
Von Mises–Fisher Distribution

The VMF distribution ($\mathcal{F}$) is one of the most commonly used distributions for modeling directional data [70]. Surface normal vectors lie over the $\mathbb{S}^3$ sphere under the VMF distribution. The VMF distribution is fully defined by two parameters, namely, the mean direction $\boldsymbol{\mu} \in \mathbb{S}^3$ and the concentration parameter $\kappa \in \mathbb{R}$. With a larger value for κ, the directional vectors drawn from the corresponding VMF distribution are more concentrated about $\boldsymbol{\mu} \in \mathbb{R}^3$. The VMF pdf of a random orientational vector $\boldsymbol{u} \in \mathbb{R}^3$ is formally defined as

$$p(\boldsymbol{u}|\boldsymbol{\mu}, \kappa) = \frac{\kappa}{2\pi\left(e^{\kappa} - e^{-\kappa}\right)} e^{\boldsymbol{\mu}^{\mathsf{T}}\boldsymbol{u}}. \tag{20}$$

Appendix B
Derivation of (6)

By eliminating the constants independent of Θ, we can have the expression of Θ as follows:

$$f(\Theta) = -\sum_{j=1}^{N}\sum_{i=1}^{N_j}\sum_{m=1}^{M+1} \alpha_{\mathrm{jim}} \log p(\mathbf{d}_{ji}|z_{ji} = m; \quad \Theta). \tag{21}$$

Substituting the expression of $p(\mathbf{d}_{ji}|z_{ji} = m; \Theta)$ in (3) into (21), we can have the following:

$$\begin{aligned} f(\Theta) = &-\sum_{j=1}^{N} N_{\mathbf{P}j} \log\kappa_j + \sum_{j=1}^{N} N_{\mathbf{P}j} \log\left(e^{\kappa_j} - e^{-\kappa_j}\right) \\ &- \sum_{\mathrm{jim}} \kappa_j \alpha_{\mathrm{jim}} (\mathbf{R}_j \widehat{\mathbf{y}}_m)^{\mathsf{T}} \widehat{\mathbf{x}}_{ji} + \frac{3}{2}\sum_{j=1}^{N} N_{\mathbf{P}j} \log\sigma_j^2 \\ &+ \sum_{\mathrm{jim}} \frac{1}{\sigma_j^2} \alpha_{\mathrm{jim}} \left(\mathbf{x}'_{ji}\right)^{\mathsf{T}} \mathbf{R}_j \mathbf{y}'_m \end{aligned} \tag{22}$$

where $N_{\mathbf{P}j} = \sum_{i=1}^{N_j}\sum_{m=1}^{M} \alpha_{\mathrm{jim}}$ denotes the sum of correspondence probabilities of all points in the jth PS with the mth point in the underlying model PS.

Appendix C
Explicit Expression of $\alpha_{\mathrm{jim}}^{q}$ in (8)

With (3) and (8), the explicit expression of posterior probabilities $\alpha_{\mathrm{jim}}^{q}$ is shown in (23) at the bottom of this page, where $r_j^{q-1} = \kappa_j^{q-1}/(2\pi(e^{\kappa_j^{q-1}} - e^{-\kappa_j^{q-1}})\left(4\pi(\sigma_j^2)^{q-1}\right)^{(3/2)}))$, $c = w/((1-w)(r_j^{q-1}))$.

Appendix D
Derivation of $\mathbf{R}_j^q$ in (12)

In this section, we give a detailed derivation of the expression for the optimal rotation matrix $\mathbf{R}_j^q$ in (12).

$$\alpha_{\mathrm{jim}}^{q} = \frac{e^{\frac{-1}{2\left(\sigma_j^2\right)^{q-1}}\left\|\mathbf{x}_{ji} - \left(\mathbf{R}_j^{q-1}\mathbf{y}_m^{q-1} + \mathbf{t}_j^{q-1}\right)\right\|^2 + \kappa_j^{q-1}\left(\mathbf{R}_j^{q-1}\widehat{\mathbf{y}}_m^{q-1}\right)^{\mathsf{T}}\widehat{\mathbf{x}}_{ji}}}{\sum_{s=1}^{M} e^{\frac{-1}{2\left(\sigma_j^2\right)^{q-1}}\left\|\mathbf{x}_{ji} - \left(\mathbf{R}_j^{q-1}\mathbf{y}_s^{q-1} + \mathbf{t}_j^{q-1}\right)\right\|^2 + \kappa_j^{q-1}\left(\mathbf{R}_j^{q-1}\widehat{\mathbf{y}}_s^{q-1}\right)^{\mathsf{T}}\widehat{\mathbf{x}}_{ji}} + c} \tag{23}$$

To begin with

$$\begin{aligned}\mathbf{R}_j^q &= \arg\max_{\mathbf{R}_j}\left(\frac{1}{\left(\sigma_j^2\right)^{q-1}}\sum_{i=1}^{N_j}\sum_{m=1}^{M}\alpha_{\mathrm{jim}}^q\left(\left(\mathbf{x}'_{ji}\right)^q\right)^{\mathsf{T}}\mathbf{R}_j\left(\mathbf{y}'_{m,j}\right)^q\right.\\ &\qquad\left.+\kappa_j^{q-1}\sum_{i=1}^{N_j}\sum_{m=1}^{M}\alpha_{\mathrm{jim}}^q\left(\mathbf{R}_j\widehat{\mathbf{y}}_m^{q-1}\right)^{\mathsf{T}}\widehat{\mathbf{x}}_{ji}\right)\\ &= \arg\max_{\mathbf{R}_j}\mathrm{Tr}\left(\frac{1}{\left(\sigma_j^2\right)^{q-1}}\sum_{i=1}^{N_j}\sum_{m=1}^{M}\alpha_{\mathrm{jim}}^q\left(\left(\mathbf{x}'_{ji}\right)^q\right)^{\mathsf{T}}\mathbf{R}_j\left(\mathbf{y}'_{m,j}\right)^q\right.\\ &\qquad\left.+\kappa_j^{q-1}\sum_{i=1}^{N_j}\sum_{m=1}^{M}\alpha_{\mathrm{jim}}^q\left(\mathbf{R}_j\widehat{\mathbf{y}}_m^{q-1}\right)^{\mathsf{T}}\widehat{\mathbf{x}}_{ji}\right). \quad (24)\end{aligned}$$

With the property $\mathrm{Tr}(\mathbf{A}+\mathbf{B}) = \mathrm{Tr}(\boldsymbol{A}) + \mathrm{Tr}(\mathbf{B})$, the above-mentioned optimization problem in (24) turns to the following:

$$\begin{aligned}&\arg\max_{\mathbf{R}_j}\left(\mathrm{Tr}\left(\frac{1}{\left(\sigma_j^2\right)^{q-1}}\sum_{i=1}^{N_j}\sum_{m=1}^{M}\alpha_{\mathrm{jim}}^q\left(\left(\mathbf{x}'_{ji}\right)^q\right)^{\mathsf{T}}\mathbf{R}_j\left(\mathbf{y}'_{m,j}\right)^q\right)\right.\\ &\qquad\left.+\mathrm{Tr}\left(\kappa_j^{q-1}\sum_{i=1}^{N_j}\sum_{m=1}^{M}\alpha_{\mathrm{jim}}^q\left(\mathbf{R}_j\widehat{\mathbf{y}}_m^{q-1}\right)^{\mathsf{T}}\widehat{\mathbf{x}}_{ji}\right)\right). \quad (25)\end{aligned}$$

We now utilize the property $\mathrm{Tr}(\mathbf{ABC}) = \mathrm{Tr}(\mathbf{CAB})$ twice and $\mathrm{Tr}(\mathbf{A}) + \mathrm{Tr}(\mathbf{B}) = \mathrm{Tr}(\mathbf{A}+\mathbf{B})$ once in both "Tr" operations in (25), and we can get that $\mathbf{R}_j^q$ equals

$$\begin{aligned}&\arg\max_{\mathbf{R}_j}\mathrm{Tr}\left(\mathbf{R}_j\left(\underbrace{\frac{1}{\left(\sigma_j^2\right)^{q-1}}\sum\nolimits_{i=1}^{N_j}\sum\nolimits_{m=1}^{M}\alpha_{\mathrm{jim}}^q\left(\mathbf{y}'_{m,j}\right)^q\left(\mathbf{x}'_{ji}\right)^{q\mathsf{T}}}_{\mathbf{H}_{1j}^q}\right.\right.\\ &\qquad\left.\left.+\underbrace{\kappa_j^{q-1}\sum\nolimits_{i=1}^{N_j}\sum\nolimits_{m=1}^{M}\alpha_{\mathrm{jim}}^q\widehat{\mathbf{y}}_m^{q-1}\widehat{\mathbf{x}}_{ji}^{\mathsf{T}}}_{\mathbf{H}_{2j}^q}\right)\right). \quad (26)\end{aligned}$$

With the notation $\mathbf{H}_j^q = \mathbf{H}_{1j}^q + \mathbf{H}_{2j}^q$, (26) becomes $\mathbf{R}_j^q = \arg\max_{\mathbf{R}_j}\mathrm{Tr}(\mathbf{R}_j\mathbf{H}_j^q)$. We now adopt the lemma in [71], which states that the orthonormal matrix $\mathbf{X}^q$ to maximize $\mathrm{Tr}(\mathbf{XH}_j)$ is $\mathbf{X}^q = \mathbf{V}_j^q(\mathbf{U}_j^q)^{\mathsf{T}}$ where $\mathbf{H}_j^q = \mathbf{U}_j^q\mathbf{S}_j^q(\mathbf{V}_j^q)^{\mathsf{T}}$. Furthermore, by making $\mathbf{X}^q$ a rotation matrix (or lie in the *special orthogonal matrix group*), we get (12).

REFERENCES

[1] Q.-Y. Zhou, J. Park, and V. Koltun, "Fast global registration," in *Proc. Eur. Conf. Comput. Vis.* Cham, Switzerland: Springer, 2016, pp. 766–782.

[2] L. Wu, X. Yang, K. Chen, and H. Ren, "A minimal poe-based model for robotic kinematic calibration with only position measurements," *IEEE Trans. Autom. Sci. Eng.*, vol. 12, no. 2, pp. 758–763, Apr. 2015.

[3] S. Song, Z. Li, H. Ren, and H. Yu, "Shape reconstruction for wire-driven flexible robots based on Bézier curve and electromagnetic positioning," *Mechatronics*, vol. 29, no. 99, pp. 28–35, Aug. 2015. [Online]. Available: https://www.sciencedirect.com/science/article/abs/pii/S0957415815000689

[4] Z. Li, L. Wu, H. Yu, and H. Ren, "Kinematic comparison of surgical tendon-driven manipulators and concentric tube manipulators," *Mechanism Mach. Theory*, vol. 107, pp. 148–165, Jan. 2017. [Online]. Available: https://www.sciencedirect.com/science/article/pii/S0094114X16302580

[5] H. Ren and P. Kazanzides, "Investigation of attitude tracking using an integrated inertial and magnetic navigation system for hand-held surgical instruments," *IEEE/ASME Trans. Mechatronics*, vol. 17, no. 2, pp. 210–217, Apr. 2010.

[6] E. C. S. Chen, B. Ma, and T. M. Peters, "Contact-less stylus for surgical navigation: Registration without digitization," *Int. J. Comput. Assist. Radiol. Surg.*, vol. 12, no. 7, pp. 1231–1241, Jul. 2017.

[7] Z. Min, H. Ren, and M. Q.-H. Meng, "TTRE: A new type of error to evaluate the accuracy of a paired-point rigid registration," in *Proc. IEEE/RSJ Int. Conf. Intell. Robots Syst. (IROS)*, Sep. 2017, pp. 953–960.

[8] G. Zheng, J. Kowal, M. A. G. Ballester, M. Caversaccio, and L.-P. Nolte, "(i) Registration techniques for computer navigation," *Current Orthopaedics*, vol. 21, no. 3, pp. 170–179, Jun. 2007.

[9] B. Maiseli, Y. Gu, and H. Gao, "Recent developments and trends in point set registration methods," *J. Vis. Commun. Image Represent.*, vol. 46, pp. 95–106, Jul. 2017.

[10] A. Rasoulian, R. Rohling, and P. Abolmaesumi, "Group-wise registration of point sets for statistical shape models," *IEEE Trans. Med. Imag.*, vol. 31, no. 11, pp. 2025–2034, Nov. 2012.

[11] N. Ravikumar, A. Gooya, S. Çimen, A. F. Frangi, and Z. A. Taylor, "Group-wise similarity registration of point sets using student's t-mixture model for statistical shape models," *Med. Image Anal.*, vol. 44, pp. 156–176, Feb. 2018.

[12] J. M. Fitzpatrick, "The role of registration in accurate surgical guidance," *Proc. Inst. Mech. Eng. H, J. Eng. Med.*, vol. 224, no. 5, pp. 607–622, 2010.

[13] H. Ren and P. Kazanzides, "A paired-orientation alignment problem in a hybrid tracking system for computer assisted surgery," *J. Intell. Robotic Syst.*, vol. 63, no. 2, pp. 151–161, 2011.

[14] H. Ren, N. V. Vasilyev, and P. E. Dupont, "Detection of curved robots using 3D ultrasound," in *Proc. IEEE/RSJ Int. Conf. Intell. Robots Syst.*, Sep. 2011, pp. 2083–2089.

[15] C. Nadeau, H. Ren, A. Krupa, and P. Dupont, "Intensity-based visual servoing for instrument and tissue tracking in 3D ultrasound volumes," *IEEE Trans. Autom. Sci. Eng.*, vol. 12, no. 1, pp. 367–371, Jan. 2015.

[16] H. Ren, W. Liu, and A. Lim, "Marker-based surgical instrument tracking using dual Kinect sensors," *IEEE Trans. Autom. Sci. Eng.*, vol. 11, no. 3, pp. 921–924, Jul. 2014.

[17] J. Wang, M. Q.-H. Meng, and H. Ren, "Towards occlusion-free surgical instrument tracking: A modular monocular approach and an agile calibration method," *IEEE Trans. Autom. Sci. Eng.*, vol. 12, no. 2, pp. 588–595, Apr. 2015.

[18] Z. Min, D. Zhu, and M. Q.-H. Meng, "Accuracy assessment of an N-ocular motion capture system for surgical tool tip tracking using pivot calibration," in *Proc. IEEE Int. Conf. Inf. Automat.*, Aug. 2016, pp. 1630–1634.

[19] J. Wang, S. Song, H. Ren, C. M. Lim, and M. Q.-H. Meng, "Surgical instrument tracking by multiple monocular modules and a sensor fusion approach," *IEEE Trans. Autom. Sci. Eng.*, vol. 16, no. 2, pp. 629–639, Apr. 2019.

[20] P. G. Batchelor, P. J. E. Edwards, and A. P. King, "3D medical imaging," in *Proc. 3D Imag., Anal. Appl.* Cham, Switzerland: Springer, 2012, pp. 445–495.

[21] G. D. Evangelidis and R. Horaud, "Joint alignment of multiple point sets with batch and incremental expectation-maximization," *IEEE Trans. Pattern Anal. Mach. Intell.*, vol. 40, no. 6, pp. 1397–1410, Jun. 2018.

[22] N. Ravikumar, A. Gooya, A. F. Frangi, and Z. A. Taylor, "Robust group-wise rigid registration of point sets using t-mixture model," *Proc. SPIE*, vol. 9784, Mar. 2016, Art. no. 97840S.

[23] J. Ma, J. Zhao, J. Tian, A. L. Yuille, and Z. Tu, "Robust point matching via vector field consensus," *IEEE Trans. Image Process.*, vol. 23, no. 4, pp. 1706–1721, Apr. 2014.

[24] J. Ma, W. Qiu, J. Zhao, Y. Ma, A. L. Yuille, and Z. Tu, "RobustL_2Estimation of transformation for non-rigid registration," *IEEE Trans. Signal Process.*, vol. 63, no. 5, pp. 1115–1129, Mar. 2015.

[25] J. Ma, J. Zhao, and A. L. Yuille, "Non-rigid point set registration by preserving global and local structures," *IEEE Trans. Image Process.*, vol. 25, no. 1, pp. 53–64, Jan. 2016.

[26] J. Ma, J. Zhao, J. Tian, X. Bai, and Z. Tu, "Regularized vector field learning with sparse approximation for mismatch removal," *Pattern Recognit.*, vol. 46, no. 12, pp. 3519–3532, 2013.

[27] J. Ma, J. Zhao, J. Jiang, H. Zhou, and X. Guo, "Locality preserving matching," *Int. J. Comput. Vis.*, vol. 127, no. 5, pp. 512–531, May 2019. doi: 10.1007/s11263-018-1117-z.
[28] J. Hermans, D. Smeets, D. Vandermeulen, and P. Suetens, "Robust point set registration using EM-ICP with information-theoretically optimal outlier handling," in *Proc. CVPR*, Jun. 2011, pp. 2465–2472.
[29] F. Pomerleau, F. Colas, R. Siegwart, and S. Magnenat, "Comparing ICP variants on real-world data sets," *Auton. Robots*, vol. 34, no. 3, pp. 133–148, Apr. 2013.
[30] J. Yang, H. Li, and Y. Jia, "Go-ICP: Solving 3D registration efficiently and globally optimally," in *Proc. IEEE Int. Conf. Comput. Vis.*, Dec. 2013, pp. 1457–1464.
[31] A. V. Segal, D. Haehnel, and S. Thrun, "Generalized-ICP," *Robot., Sci. Syst.*, vol. 2, no. 4, p. 435, Jun. 2009.
[32] L. Maier-Hein *et al.*, "Convergent iterative closest-point algorithm to accomodate anisotropic and inhomogenous localization error," *IEEE Trans. Pattern Anal. Mach. Intell.*, vol. 34, no. 8, pp. 1520–1532, Aug. 2012.
[33] S. D. Billings, E. M. Boctor, and R. H. Taylor, "Iterative most-likely point registration (IMLP): A robust algorithm for computing optimal shape alignment," *PLoS ONE*, vol. 10, no. 3, 2015, Art. no. e0117688.
[34] S. Billings and R. Taylor, "Iterative most likely oriented point registration," in *Proc. Int. Conf. Med. Image Comput. Comput.-Assist. Intervent.* Cham, Switzerland: Springer, 2014, pp. 178–185.
[35] S. Billings and R. Taylor, "Generalized iterative most likely oriented-point (G-IMLOP) registration," *Int. J. Comput. Assist. Radiol. Surg.*, vol. 10, no. 8, pp. 1213–1226, 2015.
[36] B. Eckart, K. Kim, A. Troccoli, A. Kelly, and J. Kautz, "MLMD: Maximum likelihood mixture decoupling for fast and accurate point cloud registration," in *Proc. Int. Conf. 3D Vis.*, Oct. 2015, pp. 241–249.
[37] A. Myronenko and X. Song, "Point set registration: Coherent point drift," *IEEE Trans. Pattern Anal. Mach. Intell.*, vol. 32, no. 12, pp. 2262–2275, Dec. 2010.
[38] R. Horaud, F. Forbes, M. Yguel, G. Dewaele, and J. Zhang, "Rigid and articulated point registration with expectation conditional maximization," *IEEE Trans. Pattern Anal. Mach. Intell.*, vol. 33, no. 3, pp. 587–602, Mar. 2011.
[39] W. Tao and K. Sun, "Asymmetrical Gauss mixture models for point sets matching," in *Proc. IEEE Conf. Comput. Vis. Pattern Recognit.*, Jun. 2014, pp. 1598–1605.
[40] B. Jian and B. C. Vemuri, "Robust point set registration using Gaussian mixture models," *IEEE Trans. Pattern Anal. Mach. Intell.*, vol. 33, no. 8, pp. 1633–1645, Aug. 2011.
[41] X. Kang, W.-P. Yau, and R. H. Taylor, "Simultaneous pose estimation and patient-specific model reconstruction from single image using maximum penalized likelihood estimation (MPLE)," *Pattern Recognit.*, vol. 57, pp. 61–69, Sep. 2016.
[42] N. Baka, C. T. Metz, C. J. Schultz, R. J. van Geuns, W. J. Niessen, and T. van Walsum, "Oriented Gaussian mixture models for nonrigid 2D/3D coronary artery registration," *IEEE Trans. Med. Imag.*, vol. 33, no. 5, pp. 1023–1034, May 2014.
[43] Z. Min, J. Wang, and M. Q.-H. Meng, "Robust generalized point cloud registration using hybrid mixture model," in *Proc. IEEE Int. Conf. Robot. Automat. (ICRA)*, May 2018, pp. 4812–4818.
[44] Z. Min and M. Q.-H. Meng, "Robust generalized point set registration using inhomogeneous hybrid mixture models via expectation maximization," in *Proc. IEEE Int. Conf. Robot. Automat. (ICRA)*, to be published.
[45] Z. Min, J. Wang, S. Song, and M. Q.-H. Meng, "Robust generalized point cloud registration with expectation maximization considering anisotropic positional uncertainties," in *Proc. IEEE/RSJ Int. Conf. Intell. Robots Syst. (IROS)*, Oct. 2018, pp. 1290–1297.
[46] G. Blais and M. D. Levine, "Registering multiview range data to create 3D computer objects," *IEEE Trans. Pattern Anal. Mach. Intell.*, vol. 17, no. 8, pp. 820–824, Aug. 1995.
[47] T. Masuda and N. Yokoya, "A robust method for registration and segmentation of multiple range images," *Comput. Vis. Image Understand.*, vol. 61, no. 3, pp. 295–307, 1995.
[48] Y. Chen and G. Medioni, "Object modeling by registration of multiple range images," *Image Vis. Comput.*, vol. 10, no. 3, pp. 145–155, Apr. 1992.
[49] V. M. Govindu, "Combining two-view constraints for motion estimation," in *Proc. IEEE Comput. Soc. Conf. Comput. Vis. Pattern Recognit. (CVPR)*, Dec. 2001, p. 2.
[50] R. Hartley, J. Trumpf, Y. Dai, and H. Li, "Rotation averaging," *Int. J. Comput. Vis.*, vol. 103, no. 3, pp. 267–305, Jul. 2013.
[51] V. M. Govindu and A. Pooja, "On averaging multiview relations for 3D scan registration," *IEEE Trans. Image Process.*, vol. 23, no. 3, pp. 1289–1302, Mar. 2014.
[52] Z. Li, J. Zhu, K. Lan, C. Li, and C. Fang, "Improved techniques for multi-view registration with motion averaging," in *Proc. 2nd Int. Conf. 3D Vis.*, vol. 1, Dec. 2014, pp. 713–719.
[53] J. Goldberger, "Registration of multiple point sets using the em algorithm," in *Proc. 7th IEEE Int. Conf. Comput. Vis.*, vol. 2, Sep. 1999, pp. 730–736.
[54] H. Badino, D. Huber, Y. Park, and T. Kanade, "Fast and accurate computation of surface normals from range images," in *Proc. IEEE Int. Conf. Robot. Automat.*, May 2011, pp. 3084–3091.
[55] K. Jordan and P. Mordohai, "A quantitative evaluation of surface normal estimation in point clouds," in *Proc. IEEE/RSJ Int. Conf. Intell. Robots Syst.*, Sep. 2014, pp. 4220–4226.
[56] X. Liu, H. Cevikalp, and J. M. Fitzpatrick, "Marker orientation in fiducial registration," *Proc. SPIE*, vol. 5032, pp. 1176–1186, May 2003.
[57] M. Charlebois, K. Gupta, and S. Payandeh, "Shape description of general, curved surfaces using tactile sensing and surface normal information," in *Proc. Int. Conf. Robot. Automat.*, vol. 4, Apr. 1997, pp. 2819–2824.
[58] T. Tsujimura and T. Yabuta, "A tactile sensing method for employing force/torque information through insensitive probes," in *Proc. IEEE Int. Conf. Robot. Automat.*, May 1992, pp. 1315–1320.
[59] N. Nakao, M. Kaneko, N. Suzuki, and K. Tanie, "A finger shaped tactile sensor using an optical waveguide," in *Proc. 16th Annu. Conf. IEEE Ind. Electron. Soc.*, vol. 1, Nov. 1990, pp. 300–305.
[60] F. Bernard, J. Thunberg, P. Gemmar, F. Hertel, A. Husch, and J. Goncalves, "A solution for multi-alignment by transformation synchronisation," in *Proc. IEEE Conf. Comput. Vis. Pattern Recognit.*, Jun. 2015, pp. 2161–2169.
[61] Z. Min, H. Ren, and M. Q.-H. Meng, "Estimation of surgical tooltip tracking error distribution in coordinate reference frame involving pivot calibration uncertainty," *Healthcare Technol. Lett.*, vol. 4, no. 5, pp. 193–198, 2017.
[62] Z. Min and M. Q.-H. Meng, "General first-order TRE model when using a coordinate reference frame for rigid point-based registration," in *Proc. IEEE 14th Int. Symp. Biomed. Imag.*, Apr. 2017, pp. 169–173.
[63] E. C. S. Chen, A. J. McLeod, J. S. H. Baxter, and T. M. Peters, "Registration of 3D shapes under anisotropic scaling," *Int. J. Comput. Assist. Radiol. Surg.*, vol. 10, no. 6, pp. 867–878, 2015.
[64] Z. Yaniv, "Registration for orthopaedic interventions," in *Proc. Comput. Radiol. Orthopaedic Intervent.* Cham, Switzerland: Springer, Sep. 2015, pp. 41–70.
[65] N. Ravikumar, "A probabilistic framework for statistical shape models and atlas construction: Application to neuroimaging," Ph.D. dissertation, Dept. Mech. Eng., Univ. Sheffield, Sheffield, U.K., 2017.
[66] Z. Min, J. Wang, and M. Q.-H. Meng, "Joint registration of multiple generalized point sets," in *Proc. Int. Workshop Shape Med. Imag.* Cham, Switzerland: Springer, Nov. 2018, pp. 169–177.
[67] C. M. Bishop, *Pattern Recognition and Machine Learning*. Cham, Switzerland: Springer, 2006.
[68] P. J. Besl and D. N. McKay, "A method for registration of 3-D shapes," *IEEE Trans. Pattern Anal. Mach. Intell.*, vol. 14, no. 2, pp. 239–256, Feb. 1992.
[69] T. M. Nguyen and Q. M. J. Wu, "Multiple kernel point set registration," *IEEE Trans. Med. Imag.*, vol. 35, no. 6, pp. 1381–1394, Jun. 2016.
[70] A. Banerjee, I. S. Dhillon, J. Ghosh, and S. Sra, "Clustering on the unit hypersphere using von Mises-Fisher distributions," *J. Mach. Learn. Res.*, vol. 6, pp. 1345–1382, Sep. 2005.
[71] K. S. Arun, T. S. Huang, and S. D. Blostein, "Least-squares fitting of two 3-D point sets," *IEEE Trans. Pattern Anal. Mach. Intell.*, vol. PAMI-9, no. 5, pp. 698–700, Sep. 1987.

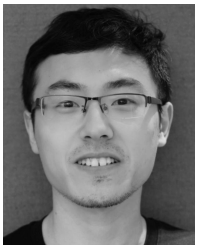

Zhe Min (S'15) received the B.S. degree in control science and engineering from Shandong University, Jinan, China, in 2014. He is currently pursuing the Ph.D. degree with the Department of Electronic Engineering, The Chinese University of Hong Kong (CUHK), Hong Kong.

His current research interests include surgical navigation, medical robotics, and surface registration algorithm.

Mr. Min was a recipient of the IROS 2017 Travel Award and the ICRA 2019 Travel Award from the IEEE Robotics and Automation Society and the International Society for Computer Aided Surgery (ISCAS) Travel Award to attend the Computer Assisted Radiology and Surgery (CARS) 2018 Congress.

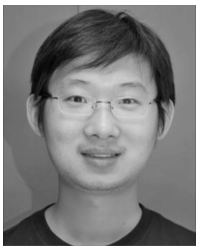

Jiaole Wang (M'15) received the B.E. degree in mechanical engineering from Beijing Information Science and Technology University, Beijing, China, in 2007, the M.E. degree from the Department of Human and Artificial Intelligent Systems, University of Fukui, Fukui, Japan, in 2010, and the Ph.D. degree from the Department of Electronic Engineering, The Chinese University of Hong Kong, Hong Kong (CUHK), in 2016.

He is currently a Research Fellow with the Pediatric Cardiac Bioengineering Laboratory, Department of Cardiovascular Surgery, Boston Children's Hospital, Harvard Medical School, Boston, MA, USA. His current research interests include medical and surgical robotics, image-guided surgery, human–robot interaction, and magnetic tracking and actuation for biomedical applications.

Dr. Wang received the Best Paper Award from the 2014 IEEE International Conference on CYBER Technology in Automation, Control, and Intelligent Systems, Hong Kong, in 2014.

Max Q.-H. Meng (M'92–F'07) received the Ph.D. degree in electrical and computer engineering from the University of Victoria, Victoria, BC, Canada, in 1992.

He was the Director of the Advanced Robotics and Teleoperation (ART) Laboratory and a Professor with the Department of Electrical and Computer Engineering, University of Alberta, Edmonton, AB, Canada, for ten years. He has been a Professor of electronic engineering with The Chinese University of Hong Kong (CUHK), Hong Kong, since 2002. He is currently the Chair of the Department of Electronic Engineering, CUHK. He is also a Distinguished Professor with the State Key Laboratory of Robotics and Systems, Harbin Institute of Technology, Harbin, China, a Distinguished Provincial Professor with the Henan University of Science and Technology, Luoyang, China, and the Honorary Dean of the School of Control Science and Engineering, Shandong University, Jinan, China. He has authored over 500 journal and conference papers. His current research interests include robotics, perception and sensing, human–robot interaction, active medical devices, biosensors and sensor networks, and adaptive and intelligent systems.

Dr. Meng is an elected member of the Administrative Committee of the IEEE Robotics and Automation Society. He is a fellow of the Hong Kong Institution of Engineers and the Canadian Academy of Engineering. He was a recipient of the IEEE Millennium Medal. He has served on many editorial boards.